

## ENGINE KNOCK PREDICTIONS USING A FULLY-DETAILED AND A REDUCED CHEMICAL KINETIC MECHANISM

J. S. COWART, J. C. KECK, AND J. B. HEYWOOD

*Massachusetts Institute of Technology  
Cambridge, MA 02139*

AND

C. K. WESTBROOK AND W. J. PITZ

*Lawrence Livermore National Laboratory  
Livermore, CA 94550*

Two chemical kinetic models are used to interpret engine knock data obtained in a laboratory internal combustion engine. These consisted of a detailed kinetic model and a reduced kinetic model, both calibrated to describe engine conditions. Comparisons of both models with experimental results are discussed. Relationships between the reaction steps of the detailed and reduced models are examined in detail, and the relative strengths and weaknesses of the two approaches are discussed.

### Introduction

Two distinctly different numerical modeling approaches have emerged in recent years for studying chemical kinetic factors related to engine knock. The present paper describes, for the first time, the application of both types of model to the same engine data. The first model of the chemical kinetics of hydrocarbon fuel autoignition in knocking engines was the so-called Shell Model,<sup>1</sup> developed at the Thornton Research Centre. The Shell Model was made more explicit first by Cox and Cole,<sup>2</sup> and then by Keck and co-workers<sup>3,4</sup> who included additional chemical pathways and a more accurate thermal analysis. This approach treats autoignition as a series of global reactions, most of which represent families of individual elementary reactions. Only those reaction paths having a direct impact on the time of occurrence of autoignition are included. As a result of these simplifications, only a small number of overall reactions are needed.

This approach is ideal in those cases where a complex, perhaps multidimensional numerical model is to be used, in which the autoignition chemistry is only a part of a larger model. The reduced kinetics submodel is computationally efficient and, when properly calibrated, correctly predicts the response of the chemical processes to modest changes in engine operating conditions and cycle-to-cycle variations.

Model calibration is accomplished for a given fuel by setting the rates and/or equilibrium constants of a few of the sensitive reactions in the reduced model

with results from combustion bomb and rapid compression machine studies. These calibrations really represent suitable averages of the rates of many elementary reactions which have been replaced by a single step in the reduced model. All other parts of the reduced model are invariant from one fuel to another.

The second, somewhat more recent modeling technique developed to study engine knock chemistry is a detailed approach which attempts to follow all of the elementary reactions taking place.<sup>5-8</sup> This is much more costly in computational terms, since it requires the model often to consider at least 10 times as many chemical species and 50 times as many reactions as the reduced approach. As such, the detailed model is generally inappropriate for inclusion in multidimensional engine models. Because the detailed modeling approach deals with elementary reactions and actual molecular structure without need for averaging processes, it has the potential for providing a very fundamental and predictive modeling tool. It also offers the possibility of dealing with fuel mixtures and kinetically-motivated additives directly, without further calibration studies. Finally, the detailed approach could be used to generate the averaged properties to be used in a reduced model.

In the present paper, both model approaches are used to examine pressure-time data taken from a test engine operated at MIT. This engine was run with both *n*-pentane and iso-octane as fuels, for initial conditions which produced knocking operation.

### Reduced Chemical Kinetic Model

The nineteen reactions included in the reduced kinetic model are listed in Table I along with Arrhenius parameters for the equilibrium and rate constants. An essential feature of this model is its ability to reproduce two-stage hydrocarbon ignition characteristics in the high pressure and low temperature region.<sup>3</sup> Some of the species, including OH, O<sub>2</sub>, HO<sub>2</sub>, HOOH, and to some extent the fuel RH, are "real" chemical species, while others, like R and RO<sub>2</sub>, represent families or groups of species. Similarly, reactions 9 and 10 and their rate expressions are taken directly from detailed modeling studies of hydrogen oxidation, while most of the other reactions represent families of reactions. Values of parameters in Table I are based on experimental data and estimates made by Benson<sup>9</sup> and are the same as those used previously by Hu and Keck.<sup>3</sup> Forward and reverse rate constants  $k^+$  and  $k^-$  are related to the equilibrium constant K by detailed balancing.

Hu and Keck<sup>3</sup> found that the simplest and most

rational way to include the effects of variations in fuel size and structure in this reduced mechanism was to adjust the equilibrium constant of reaction 3 (the isomerization reaction for the alkylperoxy radical) by changing the forward rate constant  $k_3^+$ . The reverse rate expression  $k_3^-$  and the rates of all other reactions in the model are expected to be relatively insensitive to fuel type and are kept constant. As also observed in the detailed reaction mechanism, rates of isomerization of these radicals do indeed depend rather strongly on the size and structure of the fuel molecule, and this fact, combined with the observed sensitivity of the reduced model to variations in this reaction rate, made it a convenient means of calibrating the model for different fuels.

### Detailed Chemical Kinetic Model

The numerical model used in this study is the HCT code,<sup>12</sup> which solves the coupled kinetics and energy equations. The chemical kinetic reaction

TABLE I  
Chemical kinetic model

Arrhenius parameters for the equilibrium constant  $K = A \exp(-E/RT)$  and rate constants  $k^+ = A^+ \exp(-E^+/RT)$  for *n*-pentane and iso-octane oxidation at  $700 < T < 1300$  K. The rate parameters are given in cm<sup>3</sup>-mole-sec-kcal units. Sensitivity results are given for iso-octane autoignition.

Reaction	$\Delta H_{300}$	log A	E	log A <sup>+</sup>	E <sup>+</sup>	log A <sup>-</sup>	E <sup>-</sup>	$\Delta(^{\circ}\text{CA})$
1. RH + O <sub>2</sub> = R + HO <sub>2</sub>	46.4	1.5	46.0	13.5	46.0	12.0	0	-1.0
2. R + O <sub>2</sub> = RO <sub>2</sub>	-31.0	-1.4	-27.4	12.0	0.0	13.4	27.4	0.0
3. RO <sub>2</sub> = ROOH (iso-octane)	7.5	0.0	9.8	11.0	20.8	11.0	11.0	-0.2
( <i>n</i> -pentane)	7.5	0.2	8.6	11.2	19.6	11.0	11.0	-10.6 <sup>a</sup>
4. ROOH + O <sub>2</sub> = O <sub>2</sub> RO <sub>2</sub> H	-31.0	-1.9	27.4	11.5	0.0	13.4	27.4	-0.3
5. O <sub>2</sub> RO <sub>2</sub> H = OROOH + OH	-26.6			11.3	17.0			-0.2
6. OH + RH = R + H <sub>2</sub> O	-23.5			13.3	3.0			0.0
7. OROOH = OH + ORO	43.0			15.6	43.0			0.0
8. R + O <sub>2</sub> = HO <sub>2</sub> + C = C	-13.5	0.0	-13.5	11.5	6.0	11.5	19.5	0.6
9. HO <sub>2</sub> + HO <sub>2</sub> = HOOH + O <sub>2</sub>	-38.5			12.3	0.0			-0.1
10. HOOH + M = 2OH + M	51.4			17.1	46.0			-9.2
11. ORO = R'CHO + R''O	8.5			14.0	15.0			0.0
12. RO <sub>2</sub> + HO <sub>2</sub> = ROOH + O <sub>2</sub>	-38.5			12.0	0.0			0.1
13. ROOH = OH + R'CHO + C = C	-3.0			14.4	31.0			-0.3
14. RO <sub>2</sub> + R'CHO = ROOH + R'CO	-0.6			11.45	8.6			0.0
15. RO <sub>2</sub> + RH = R + ROOH	8.0	1.1	8.0	11.2	16.0	10.1	8.0	0.0
16. HO <sub>2</sub> + R'CHO = HOOH + R'CO	-0.6			11.7	8.6			0.0
17. HO <sub>2</sub> + RH = R + HOOH	8.0	0.9	8.0	11.7	16.0	10.8	8.0	-1.2
18. HO <sub>2</sub> + C = C = Epox + OH	-0.23			10.95	10.0			0.0
19. R + R = RH	-85.0			13.2	0.0			0.1

NOTE: ROOH is grouped with OROOH and R'CO is grouped with R''O.

<sup>a</sup>Only the forward rate constant,  $k^+$ , was multiplied by 2.0.

mechanism used in the present work was based on previous studies of oxidation of large hydrocarbon fuel molecules, particularly *n*-heptane, *n*-octane, and iso-octane.<sup>5,7,13</sup> This mechanism consists of 324 species and 1303 reactions<sup>14</sup> and is too extensive to be included here.

The detailed reaction mechanism includes initiation reactions, site-specific abstraction of H atoms for each type of fuel molecule, consumption of the resulting alkyl radicals, and oxidation of the smaller hydrocarbon fragments, particularly olefins, to final products. Under engine knock conditions, addition of O<sub>2</sub> to alkyl radicals, followed by alkylperoxy isomerization and formation of epoxide intermediates are also very important reaction sequences. Many of these steps have been included in earlier models for iso-octane,<sup>5</sup> but no previous engine knock chemistry mechanism existed for *n*-pentane. A high temperature reaction mechanism for *n*-pentane<sup>15</sup> was extended to low temperature conditions to carry out the present computations, using principles discussed by Pollard<sup>11</sup> and implemented in our previous work.<sup>5,7</sup>

### Experimental Equipment and Procedure

The experimental engine data were obtained at MIT's Sloan Automotive Laboratory, using the Ricardo Hydra Mark III single-cylinder spark-ignition research engine with a 8.18:1 compression ratio. Further details on the combustion chamber configuration and the experimental equipment are given in References 4 and 14. The engine was operated at 1500 rpm, using iso-octane and *n*-pentane as fuels, with research octane numbers (RON) of 100 and 62, respectively. Ignition spark timing advance was 40° BTDC (Before Top Dead Center) for iso-octane and 32° BTDC for *n*-pentane, adjusted for both fuels to achieve knocking operation. In addition, with the very knock-resistant iso-octane, the intake fuel mixture was preheated, and the engine run at wide open throttle to promote knocking operation. With knock-prone *n*-pentane, the inlet mixture was not preheated, and the inlet pressure was reduced to roughly 0.6 atm, such that severe knock and engine damage would not occur.

Pressure was sampled at two rates, once per crank angle during most of the engine cycle, then at approximately 11 times per crank angle from slightly before top dead center to about thirty degrees after TDC during the combustion portion of the cycle. From hundreds of experimental engine cycle pressure histories, the crank angle at which knock occurred could be determined for knocking cycles, using a pressure jump criterion. It is this experimental knock point with which the predictions of the two chemical kinetic models are compared.

### Modeling Knock Onset in a Spark Ignition Engine

Smoothed pressure histories from the Ricardo engine were used to simulate the increase in pressure that the unburned gas experiences in the engine due to piston compression and burned gas expansion. In the models, the end gas is represented as a homogeneous fuel-air mixture that is compressed and expanded according to these smoothed pressure curves, and a resulting unburned gas temperature history is calculated. The knock occurrence criterion used in this study was a rate of temperature rise equal to  $6 \times 10^5$  K/sec. In this model, knock is assumed to be the result of homogeneous autoignition of the end gas. Heat transfer from the end gas to the wall and piston blowby are included only in the way they reduce the measured pressure used to compress the end gas.

All calculations were started at 90° BTDC in the compression stroke. The initial end-gas temperature, which is roughly equal to the wall temperature, is calculated by the equation of state,  $T = pV/mR$ , where  $p$ ,  $V$ , and  $m$  are measured quantities. Evaluation of the mass  $m$  requires a reliable value for the residual mass fraction from the previous cycle. A fast response (2 ms), flame ionization detector<sup>16</sup> with a sampling tube attached to the side of the spark plug provided estimates of 7 percent residual burned mass fraction at wide open throttle in the iso-octane experiments, and 20 percent at 0.6 atm inlet pressure in the *n*-pentane experiments. These values and the air and fuel mass flow rates were used to calculate the initial mass,  $m$ , which was then used to calculate the initial temperature from the equation of state. A change in the modeled residual fraction of 1% would change the initial temperature by approximately 6 K, corresponding to a noticeable change in knock prediction. The initial temperatures resulting from this analysis and used in this study were 492 K for iso-octane and 444 K for *n*-pentane.

The residual gas fraction also affects the initial gas mixture composition. In the reduced model, the residual gas was simulated as a single inert constituent, while in the detailed model the residual burned gas was included as a mixture of CO, CO<sub>2</sub>, H<sub>2</sub>, H<sub>2</sub>O and O<sub>2</sub>.

To remove a bias towards forced ignition, the pressure data were smoothed and the discontinuous changes in slope of the pressure records, which signal the occurrence of knock, were eliminated. This procedure is inexact and potential errors introduced thereby have been discussed previously by Green et al.<sup>10</sup> This practice essentially assumes that the measured pressure history results entirely from bulk gas combustion and is not influenced by heat release in the end gas. This is reasonably accurate for small end-gas mass fractions.

As noted previously by Chun et al.,<sup>4</sup> cycle-to-cycle variations at fixed engine operation contributed considerably to variation in time of knock occurrence in this engine, with measured knock being observed at times from 0.5° BTDC to 5.5° ATDC for iso-octane and from 8–20° ATDC for *n*-pentane. This variability occurs, even though operating parameters such as air/fuel ratio, engine speed, spark timing, and initial temperature and pressure remain fixed for each fuel. Individual pressure histories over these ranges were then used to drive the kinetic models, using the same pressure histories for both models, and the computed times of knock occurrence were compared with the observed times.

### Modeling Results

#### *Iso-octane:*

Both models were used first to simulate the experimental results for iso-octane. In spite of the complexity of this fuel, previous studies by Hu and Keck<sup>3</sup> and by Chun et al.,<sup>4</sup> using the reduced kinetic model, and by Westbrook et al.<sup>5</sup> with a detailed kinetic model, simulated engine knock problems with iso-octane reasonably well.

Initial results for the reduced model, using rate expressions from Table I and values for  $A_3$  and  $E_3$  from Ref. 3, gave times of knock occurrence that were too late. The reduced model was recalibrated by decreasing the value of  $E_3^+$  from its initial value of 22.4 kcal/mole to a value of 20.8 kcal/mole and leaving the pre-exponential term  $A_3$  unchanged. The sensitivity of the computed results to variation in this rate was sufficient to accelerate the computed rate of autoignition to agree with the experiments. The resulting numerical predictions are summarized as the open circles in Fig. 1, showing good agreement between predicted and measured times of knock occurrence. Perfect agreement would place the computed results along the diagonal line. Also plotted on Fig. 1 are the results for the detailed model (solid circles). They are slightly later than the experimental observations.

It is important to recall the procedure used originally to calibrate the reduced model. Constant volume combustion bomb results were the major components in this calibration, conditions which can be quite far removed from those encountered in knocking engines. The present results showed that calibration of the model from bomb results alone is not sufficiently accurate to ensure reliable prediction of engine performance. The reduced model must be recalibrated for each fuel under engine conditions related to the problem of interest. However, only one pressure history from the large body of iso-octane engine data was needed to accomplish

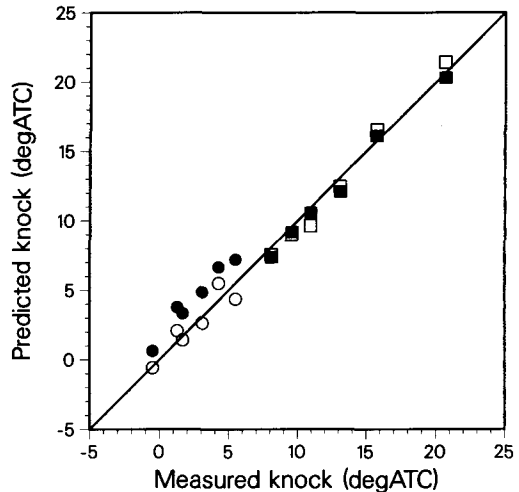


FIG. 1. Predicted times of knock occurrence, plotted against experimentally measured values. Open symbols show reduced kinetic model results, and solid symbols show results from detailed kinetic model. The circles refer to iso-octane and the squares to *n*-pentane.

this calibration, so that all but one of the open circles in Fig. 1 represent predictive calculations with the reduced kinetic model.

Temperature and OH concentration profiles for one of the pressure histories are shown in Fig. 2, with results from the reduced model shown as the dashed curve and results from the detailed model as the solid curve. The profiles indicate two-stage ignition behavior common to such problems. The

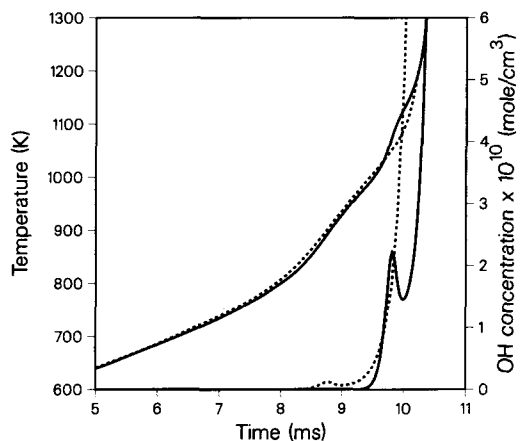


FIG. 2. Temperature and OH concentration histories when iso-octane is the fuel. The dashed curves refer to the reduced model and the solid curves to the detailed kinetic model.

OH profile is shown since OH is the primary radical that consumes the fuel and intermediate species and produces heat release through formation of water. This heat release raises the end-gas temperature and furthers the progress of the end gas towards autoignition.

#### *n*-Pentane:

The second set of engine data treated *n*-pentane as the fuel. This fuel, with its octane value of 62 RON, is qualitatively much different from iso-octane. In the reduced model, the original value<sup>3</sup> of  $E_3^+$  was reduced slightly from 8.8 kcal/mole to 8.6 kcal/mole to obtain good agreement. As shown in Fig. 1, the reduced (open squares) and detailed (solid squares) models show excellent agreement with the experimental results. The squares are close to the diagonal line and reflect the correct slope.

#### Relationships Between Reduced and Detailed Kinetic Models

Many of the reactions in the reduced model are taken directly from the detailed model. The elementary reactions 9 and 10 (Table I) are equivalent in both models. The initiation reaction 1 is also very comparable to the same step in a detailed model, and is important only for a very short period of time during the ignition time. The process of H-atom abstraction from the fuel, reactions 6, 15, and 17, are modeled closely on the same processes in the detailed model, with the reaction rates from the reduced model being approximately equal to the detailed H-atom abstraction steps.

A careful sensitivity analysis was carried out for the reduced reaction mechanism, in which each reaction rate was systematically varied, one at a time, by a factor of two, and the resulting autoignition records were compared with the results from the baseline model. The results of this comparison in the case of iso-octane are summarized in the last column of Table I, showing the difference in crank angle position ( $\Delta$ ) at which knock was observed when the reaction rate was increased by a factor of two, compared to the time of knock occurrence in the baseline mechanism. A negative value of  $\Delta$  means that knock occurrence was moved to earlier times. The greatest sensitivity to a change in rate constant was found to be to reaction 10, the dissociation of HOOH to produce 2 OH radicals. An increase in rate of this reaction, which is explicitly based on the detailed reaction mechanism, resulted in a much earlier time of knock occurrence. Note that we assumed a low pressure limit rate expression for reaction 10 in both models. A recent review of Tsang<sup>20</sup> shows that this reaction does exhibit some fall-off behavior for pressures above 10 atm. Correcting for

fall-off, the rate is about 40% slower at 40 atm and 1000 K, typical conditions at which the fuel is rapidly consumed during autoignition.

Next highest in sensitivity is reaction 17, which adds to the production of HOOH. Increases in the rates of both reactions 10 and 17 result in a faster rate of OH production and earlier ignition times. Reaction 1 also has a significant degree of sensitivity, since production of HO<sub>2</sub> radicals leads to the production of more OH radicals. There is no computed sensitivity to the rate of reaction 2, although it is the key step in the production of OH through alkylperoxy isomerization. The reason for this apparent insensitivity is the fact that, in this model, this step is closely equilibrated. In the sensitivity analysis, both the forward and reverse reaction rates were doubled, so the equilibrium constants were unaffected. However when the equilibrium constant of reaction 2 was doubled (by modifying the forward rate constant), a large sensitivity is indicated (Table I). The same procedure was followed for reaction 3, where only the forward rate constant was doubled. The sensitivity coefficient was  $-10.6$ , the largest observed, indicating why this equilibrium constant can be used as a sensitive calibration parameter in the reduced model.

In contrast, an increase in the rate of reaction 8 results in a later time of autoignition, since production of the stable intermediate species C=C slows the rate of radical growth. The RO<sub>2</sub> isomerization sequence, starting with reaction 3, accelerates the rate of ignition, both from the direct isomerization of RO<sub>2</sub> and from the production and consumption of dihydroperoxy radical species. All of these trends are very similar to those observed for the detailed kinetic mechanism.

The principal structure-dependent steps in the reduced kinetic model are the alkylperoxy isomerizations, represented by reaction 3. This generic reaction can be compared directly with the detailed reactions which it is intended to simulate, as shown in Table II, where the rate parameters are given and evaluated at 900 K. The rate parameters are based on the work of Baldwin and Walker<sup>17</sup> and have been adjusted to agree with Slagle and Gutman R + O<sub>2</sub> = RO<sub>2</sub> equilibrium constants.<sup>18,19</sup> The reverse rates are based on thermochemistry from Pollard.<sup>11</sup>

For the pentylperoxy radicals, five elementary isomerization steps are shown, but only the last two of these contribute significantly to the detailed model simulation, due to the high activation energy barriers (i.e., 30 and 26.5 kcal/mole) of the other three paths and the lower concentration of the 3C<sub>5</sub>H<sub>11</sub>O<sub>2</sub> radical. These higher energy barriers are due to the high strain energies involved in the ring-like transition state when an H atom is abstracted from the  $\alpha$  site, adjacent to the site at which the molecular oxygen is attached. In contrast, the fifth isomeri-

TABLE II

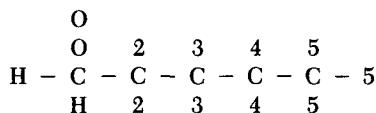
Selected RO<sub>2</sub> isomerization reactions in *n*-pentane and iso-octane reaction mechanisms, including rate parameters. Right-hand column shows rate expression evaluated at 900 K.

Reaction	A <sup>+</sup> sec <sup>-1</sup>	E <sup>+</sup> kcal/mole	k <sup>+</sup> (900 K) sec <sup>-1</sup>
<i>n</i> -Pentane:			
RO <sub>2</sub> → ROOH (reduced model)	1.585 × 10 <sup>11</sup>	21.06	2.8 × 10 <sup>6</sup>
1C <sub>5</sub> H <sub>11</sub> O <sub>2</sub> → 1C <sub>5</sub> H <sub>10</sub> OOH-2	1.5 × 10 <sup>11</sup>	26.5	5.5 × 10 <sup>4</sup>
2C <sub>5</sub> H <sub>11</sub> O <sub>2</sub> → 2C <sub>5</sub> H <sub>10</sub> OOH-1	2.9 × 10 <sup>11</sup>	30.0	1.5 × 10 <sup>4</sup>
3C <sub>5</sub> H <sub>11</sub> O <sub>2</sub> → 3C <sub>5</sub> H <sub>10</sub> OOH-2	3.0 × 10 <sup>11</sup>	26.5	1.0 × 10 <sup>5</sup>
2C <sub>5</sub> H <sub>11</sub> O <sub>2</sub> → 2C <sub>5</sub> H <sub>10</sub> OOH-4	1.2 × 10 <sup>11</sup>	23.4	2.4 × 10 <sup>5</sup>
1C <sub>5</sub> H <sub>11</sub> O <sub>2</sub> → 1C <sub>5</sub> H <sub>10</sub> OOH-4	2.0 × 10 <sup>11</sup>	21.5	1.2 × 10 <sup>6</sup>
<i>Iso</i> -octane:			
RO <sub>2</sub> → ROOH (reduced model)	1.0 × 10 <sup>11</sup>	22.4	8.9 × 10 <sup>5</sup>
<i>a</i> C <sub>8</sub> H <sub>17</sub> O <sub>2</sub> → <i>a</i> C <sub>8</sub> H <sub>16</sub> OOH-3	1.0 × 10 <sup>11</sup>	17.9	4.5 × 10 <sup>6</sup>
<i>d</i> C <sub>8</sub> H <sub>17</sub> O <sub>2</sub> → <i>d</i> C <sub>8</sub> H <sub>16</sub> OOH-1	2.0 × 10 <sup>11</sup>	23.0	5.2 × 10 <sup>5</sup>
<i>d</i> C <sub>8</sub> H <sub>17</sub> O <sub>2</sub> → <i>d</i> C <sub>8</sub> H <sub>16</sub> OOH-3	1.2 × 10 <sup>11</sup>	23.4	2.5 × 10 <sup>5</sup>

Note that the number preceding the RO<sub>2</sub> and ROOH species name refers to the site where the O<sub>2</sub> is attached and the terminal number on the ROOH species name refers to the position of the H-atom internally abstracted. The "a" refers to one of the nine logically identical, primary sites on one end of the iso-octane molecule and the "d" refers to one of the six logically identical, primary sites on the other end.

zation reaction, 1C<sub>5</sub>H<sub>11</sub>O<sub>2</sub> = 1C<sub>5</sub>H<sub>10</sub>OOH-4 involves a 7-membered ring transition state and the 2C<sub>5</sub>H<sub>11</sub>O<sub>2</sub> = 2C<sub>5</sub>H<sub>10</sub>OOH-4 reaction involves a 6-membered ring, both of which have low or zero strain energy barriers.

We can illustrate the structural features of the 1C<sub>5</sub>H<sub>11</sub>O<sub>2</sub> isomerization reactions as follows:

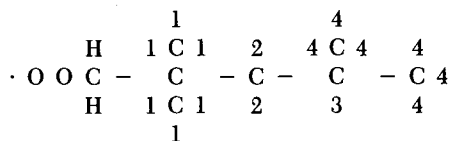


in which the numerals 2-5 indicate logically distinct H atoms in the alkylperoxy radical. The product 1C<sub>5</sub>H<sub>10</sub>OOH-4 indicates that one of the H atoms labeled '4' in this diagram has been transferred to the free site at the O atom. The now-empty '4' site is available for further addition of molecular oxygen as in reaction 4 of the reduced model (Table I), or the same product can decompose, leaving an OH radical as in reaction 13. The detailed model includes these and other paths as well, all of which can depend on structural factors.

As the size of the *n*-alkane fuel molecule increases from *n*-butane to *n*-pentane and eventually to *n*-octane, three important trends affect the overall rate of isomerization in the detailed model.<sup>7,11</sup> First, the fraction of isomerization paths which are free of strain energy barriers increases rapidly; second, the number of H atoms accessible to internal

abstraction increases; and third, the ratio of H atoms in the fuel molecule bound at primary sites, with their greater bond energy and lower rate of abstraction, to those bound at weaker secondary sites decreases. All three factors lead to faster isomerization as the molecule size increases; these factors are ultimately reflected in the reduced kinetic mechanism by a gradual reduction in E<sub>3</sub> and E<sub>3</sub><sup>+</sup> with increasing molecule size.<sup>3,4</sup>

The isomerization reactions for iso-octane are also shown in Table II. Only the three fastest isomerization reactions in the detailed model are shown. The reaction in the reduced model has a lower overall rate than for *n*-pentane. However, the corresponding reactions from the detailed kinetic model are at least as fast for iso-octane as they were for *n*-pentane. In fact, the first of the detailed reactions for iso-octane in Table II is considerably faster than any of the steps for *n*-pentane. Schematically, this fast reaction can be indicated as the internal abstraction of the '3' H atom located at the tertiary site in iso-octane,



Since this involves a relatively unstrained 7-membered intermediate ring structure, and the H

atom being abstracted is a weakly bound H atom, the process ought to be rapid, and the detailed model results reflect that fact. However, the detailed model also shows clearly that, once this internal H atom transfer is complete, the subsequent addition of another O<sub>2</sub> at the '3' site is relatively unimportant. This is due to the fact that molecular oxygen is bound less strongly at tertiary sites<sup>7</sup> than at primary and secondary sites, and the equilibrium for the addition of the second O<sub>2</sub> molecule at the tertiary site lies strongly to the dissociation side, rather than the adduct side. As a result, reaction paths leading to dihydroperoxide species and the large amounts of OH radicals produced during that process are suppressed in the detailed model in a natural way.

The reduced model, however, assumes through reaction 4 that formation of dihydroperoxide species and subsequent production of OH from reactions 5 and 7 are independent of fuel size and structure, leaving all of the structural factors to be incorporated into  $k_3^+$ . Therefore, to inhibit chain branching for iso-octane, the reduced model changes the overall influence of these processes by altering the rate of RO<sub>2</sub> isomerization.

Another difference between the reduced and detailed models is the omission in the reduced model of reactions of the type R → Olefin + R'. This generic reaction corresponds to a large set of reactions in the detailed model and becomes increasingly important at high temperatures in removing active R radicals by converting them to smaller, relatively inactive R' radicals, resulting in longer ignition delay times. Incorporation of this reaction in the reduced model and an investigation of its sensitivity would be highly desirable and is currently in progress.

A final comment relates to the comparable computing costs for the two models. The detailed model required from 10 to 30 CPU minutes per pressure history on a CRAY-XMP computer, while the reduced model requires only a few seconds on the same computer to complete a comparable engine cycle.

### Conclusions

The ultimate goal of both of these combustion modeling efforts is the development of a reliable and physically sound means of interpreting experimental data and a tool for predicting the response of a combustion system to variations in operating conditions. The above results have shown that, under controlled conditions, both models can interpret and predict experimental results. The reduced model required calibration using engine data, but was very economical in computer resources. The detailed model did not require additional calibra-

tion to simulate engine knock data, but was computationally expensive. The present results apply only to two pure fuels, and extensions of these models to mixtures of fuels are under consideration for future study.

### Acknowledgments

The computational portion of this work was supported by the U.S. Department of Energy, Division of Energy Conversion and Utilization Technologies, and was carried out by the Lawrence Livermore National Laboratory under the auspices of the U.S. Department of Energy under contract No. W-7405-ENG-48. The experimental work was sponsored by the MIT Sloan Automotive Laboratory's Consortium for Engine Research. Member companies supporting this effort were: Ford Motor Company, Chrysler Corporation, Peugeot Societe Anonyme, and Regie Nationale des Usines Renault.

### REFERENCES

1. KIRSCH, L. J., AND QUINN, C. P.: *J. Chem. Phys.* 82, 459 (1985).
2. COX, R. A., AND COLE, J. A.: *Comb. Flame* 60, 109 (1985).
3. HU, H., AND KECK, J. C.: SAE paper No. 872110 (1987).
4. CHUN, K. M., HEYWOOD, J. B., AND KECK, J. C.: *Twenty-Second Symposium (International) on Combustion*, p. 455, The Combustion Institute, Pittsburgh, 1989.
5. WESTBROOK, C. K., WARNATZ, J., AND PITZ, W. J.: *Twenty-Second Symposium (International) on Combustion*, p. 893, The Combustion Institute, Pittsburgh, 1989.
6. LEPPARD, W.: *Comb. Sci. Tech.* 43, 1 (1985).
7. WESTBROOK, C. K., AND PITZ, W. J.: SAE Trans. Section 7, 96, 559 (1988), paper No. 872107.
8. WARNATZ, J.: Numerical Simulation of Ignition Processes. Paper presented at the Third International Conference on Numerical Combustion, Antibes, France, May 1989.
9. BENSON, S. W.: *Prog. Energy Comb. Sci.* 7, 125 (1981).
10. GREEN, R. M., PARKER, C. D., PITZ, W. J., AND WESTBROOK, C. K.: SAE Trans. Section 4, 96 (1988), paper No. 870169.
11. POLLARD, R. T.: in *Comprehensive Chemical Kinetics* (C. H. Bamford and C. F. H. Tipper, Eds.), vol. 17, p. 249 (1977).
12. LUND, C. M.: HCT—A General Computer Program for Calculating Time-Dependent Phenomena Involving One-Dimensional Hydrodynamics, Transport, and Detailed Chemical Kinetics, Lawrence Livermore Laboratory report UCRL-52504, 1978.

13. AXELSSON, E., BREZINSKY, K., DRYER, F. L., PITZ, W. J., AND WESTBROOK, C. K.: Twenty-First Symposium (International) on Combustion, p. 783, The Combustion Institute, Pittsburgh, 1988.
14. COWART, J. S., KECK, J. C., HEYWOOD, J. B., WESTBROOK, C. K., AND PITZ, W. J.: Comparison of Engine Knock Predictions Using a Fully-Detailed and a Reduced Chemical Kinetic Mechanism. Paper presented at the Western States Section of The Combustion Institute, October 23-24, Livermore, CA, 1989.
15. WESTBROOK, C. K., PITZ, W. J., THORNTON, M. M., AND MALTE, P. C.: *Comb. Flame* 72, 45 (1988).
16. WAI, K., GALLIOT, F., CHENG, T. AND SZTENDEROWICZ, M.: SAE Paper No. 900485, 1990.
17. WALKER, R. W.: in *Reaction Kinetics* vol 1, p. 161, The Chemical Society, London, 1975.
18. SLAGLE, I. R., RATAJCZAK, E., HEAVEN, M. C., GUTMAN, D. AND WAGNER, A. F.: *J. Am. Chem. Soc.* 107, 1838 (1985).
19. SLAGLE, I. R., RATAJCZAK, E., AND GUTMAN, D.: *J. Phys. Chem.* 90, 402 (1986).
20. TSANG, W., AND HAMPSON, R. F.: *J. Phys. Chem. Ref. Data* 15, 1087 (1986).